SUPPORTING MATERIAL

Tomography of a Cryo-immobilized Yeast Cell using Ptychographic Coherent X-ray Diffractive Imaging

K. Giewekemeyer[1,*], C. Hackenberg[2], A. Aquila[1], R. N. Wilke[3], M. R. Groves[2], R. Jordanova[2], V. S. Lamzin[2], G. Borchers[1], K. Saksl[4], A. V. Zozulya[5], M. Sprung[5], and A. P. Mancuso[1,#]

[1]*European XFEL GmbH, Hamburg, Germany*

[2]*European Molecular Biology Laboratory Hamburg c/o DESY, Hamburg, Germany*

[3]*Institut für Röntgenphysik, Georg-August-Universität Göttingen, Göttingen, Germany*

[4]*Institute of Materials Research, Slovak Academy of Sciences, Kosice, Slovak Republic*

[5]*DESY Photon Science, Hamburg, Germany*

Correspondence: *klaus.giewekemeyer@xfel.eu, #adrian.mancuso@xfel.eu

A. Aquila's present address is Stanford Linear Accelerator Center, Menlo Park, CA.

M.R. Groves present address is Department of Pharmacy, University of Groningen, Groningen, The Netherlands.

1. ANALYSIS

1.1. Ptychographic reconstruction

The ptychographic reconstruction of the tomographic projections was initiated for each projection angle with the probe reconstruction as retrieved from the test sample data set. Each reconstruction was started with a weakly random initial seed, with pixel values defined as $(0.95 + 0.05 \cdot r_1) \cdot \exp(i\, \pi/10 \cdot r_2)$ and r_1, r_2 chosen as uniformly distributed random numbers in the interval [0,1] and [-1,1], respectively. For each projection the ePIE algorithm was evaluated for 300 iterations, averaging the complex probe and object over the last 20 iterations (1). The probe was confined by a circular mask with a diameter equal to the field of view, similar as described in (2). For both the test sample and the yeast cell dataset the amplitude was clipped to the interval [0.9,1] (3). To further aid the reconstruction, phase values were clipped to the interval $[-\pi,0]$. The feedback parameters of the ePIE algorithm (4) were chosen as $\alpha = 0.5$ (object) and $\beta = 0.25$ (probe).

1.2. Background correction

1.2.1. Simulation of a cell partially immersed into a slab of material

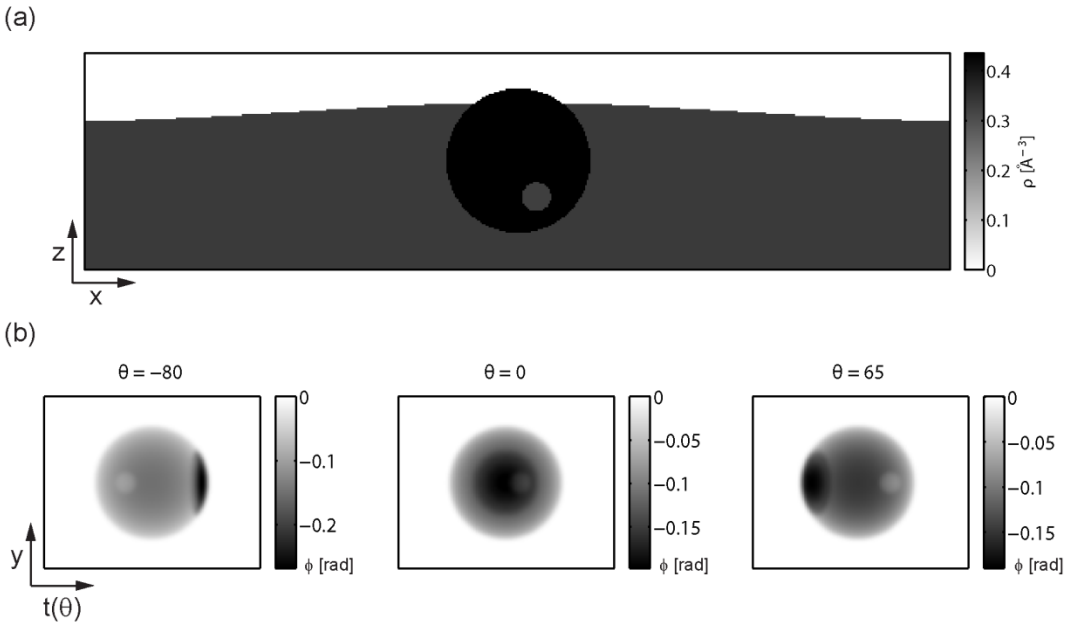

Figure S1: Model of a cell partially immersed into a slab of water with a curved surface. (a) Central slice through the 3D (electron) density distribution in a plane perpendicular to the rotation axis (along y). (b) Phase projections at three differenct projection angles, after subtraction of the inhomogeneous background and offset equalization.

To validate the empirical model that is used here for background correction of the experimental data, the 3D (electron) density distribution of a spherical cell partially immersed into a slab of water was simulated in a volume containing 128×128×2048 pixels, each with a side length of 40 nm (see Fig. S1(a)). More precisely, the cell was assumed to be partially immersed in a (nearly) plane-parallel slab of water. An inhomogeneous background contribution with a surface described by a Gaussian height distribution function (maximum height 30% of the particle radius, standard deviation of three times the particle radius) was added. A water density of 1.0 g/ml was assumed, and for the cellular material the sum formula H50C30N9O10S1 and mass density 1.35 g/ml (5) was used to determine the corresponding refractive index components (6). The photon energy was considered the same as in the experiment (7.9 keV). A small vacuole inside the cell was assigned a density of 75% times that in the remaining cellular volume. A region of interest in a central slice perpendicular to the y-axis illustrates the different density contributions (see Fig. S1(a)).

The resulting phase projections, obtained by numerical Forward Radon transformation (Matlab (7) built-in function "radon.m"), are shown in Fig. S1(b). As for the experimental

data, the inhomogeneous background contribution was subtracted here by modeling and forward projecting the density of a slab with a Gaussian height distribution profile (here the same as used for simulation). In addition, the constant offset of the phase projections was equalized for all projections. As for the experimental data, the projections were filtered by Gaussian convolution with a standard deviation of 1.5 pixels.

A main feature that can be observed in the experimental phase projections (see main text, Fig. 3), namely a characteristic region of stronger phase retardation, compared to the remainder of the cell, is also observed here. It is caused by the fraction of the cell that protrudes the water layer surrounding it. This confirms that the model used for the experimental background correction accurately describes the geometry of the sample.

1.2.2. Overall effect of the experimental background correction

The overall effect of the corrections is illustrated in Fig. S2 which shows a plot of the integrated projected phase sum $\int_{\overline{S}} \overline{\Phi}_\theta(t,y)\mathrm{d}t\mathrm{d}y$ before and after the background correction. Here $\overline{S}$ denotes the complement of the cell support in each projection. As evident from the plot the background correction brings the overall background to 0, thus leaving essentially the cell density itself as the only contribution to the phase projections.

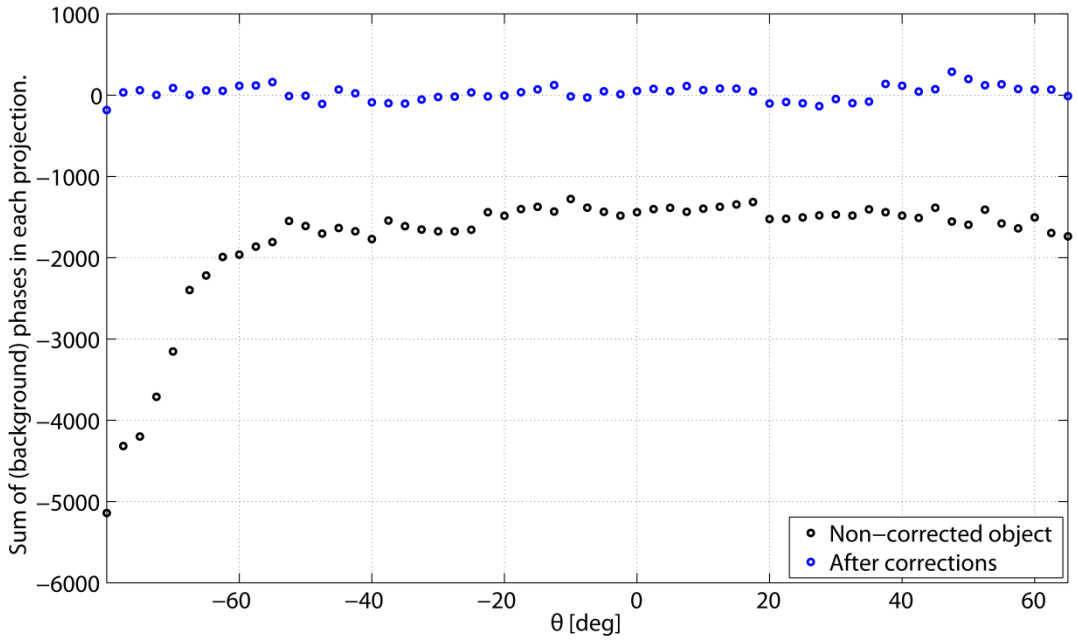

Figure S2: Effect of the background subtraction on the overall phase sum outside the cell support S, plotted against the projection angle θ. Before the background correction the values are scattered around a constant non-zero value, except for angles below -60°. After the background corrections all values are located around zero.

1.3. Tomographic reconstruction

In Figure S3 slices in a plane perpendicular to the rotation axis are shown for (a) the reconstruction from experimental data and (b) from simulated data (see above). There is a very high degree of similarity between model and experiment, indicating the validity of the model. The images show that the cell half on the opposite side of the protruding fraction is essentially unaffected by the partial submersion of the cell and remaining artifacts are due to the missing wedge.

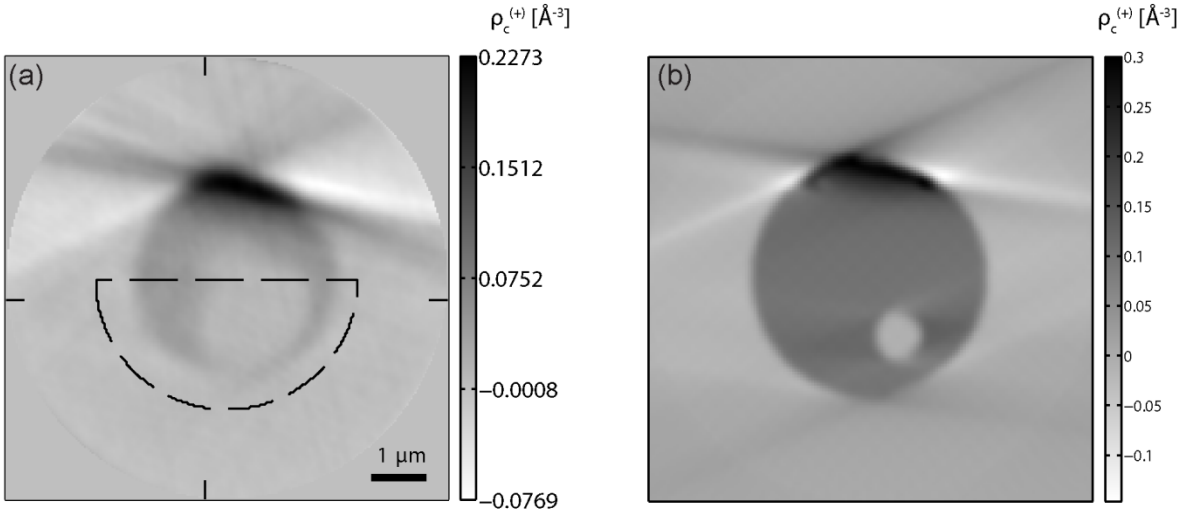

Figure S3: Slices through the reconstructed experimental (a) and simulated density distributions (b). The dashed line in subfigure (a) indicates the volume that was used for quantitative density analysis.

1.4. Resolution determination

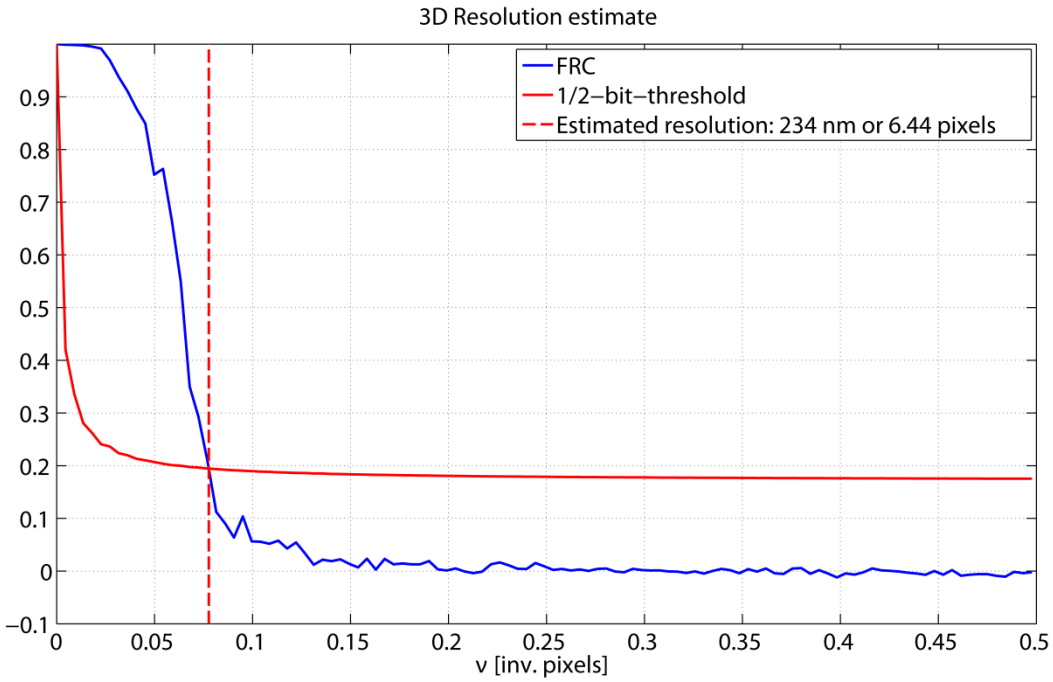

Figure S4: Azimuthally averaged Fourier-Shell-correlation curve (blue) obtained from correlating two independent tomographic reconstructions, each representing one half of the dataset. The intersection of the blue curve with the 1/2-bit threshold curve (red) marks an estimate for the obtained half-period resolution, 234 nm.

The (half-period) resolution was determined by intersecting the resulting FRC curve with the so-called 1/2-bit threshold curve. This line indicates the FRC value for each spatial frequency, at which the average information content of each voxel is 0.5 bits (8). The resulting FRC curve and the 1/2-bit threshold curve are depicted in Fig. S4. The two curves intersect at a resolution value of 234 nm.

SUPPORTING REFERENCES

1. Shapiro, D., P. Thibault, T. Beetz, V. Elser, M. Howells, C. Jacobsen, J. Kirz, E. Lima, H. Miao, A.M. Neiman, and D. Sayre. 2005. Biological imaging by soft x-ray diffraction microscopy. Proc. Natl. Acad. Sci. U. S. A. 102: 15343–15346.

2. Giewekemeyer, K., M. Beckers, T. Gorniak, M. Grunze, T. Salditt, and A. Rosenhahn. 2011. Ptychographic coherent x-ray diffractive imaging in the water window. Opt. Express. 19: 1037.

3. Wilke, R.N., M. Priebe, M. Bartels, K. Giewekemeyer, A. Diaz, P. Karvinen, and T. Salditt. 2012. Hard X-ray imaging of bacterial cells: nano-diffraction and ptychographic reconstruction. Opt. Express. 20: 19232–19254.

4. Maiden, A.M., and J.M. Rodenburg. 2009. An improved ptychographical phase retrieval algorithm for diffractive imaging. Ultramicroscopy. 109: 1256–1262.

5. Howells, M.R., T. Beetz, H.N. Chapman, C. Cui, J.M. Holton, C.J. Jacobsen, J. Kirz, E. Lima, S. Marchesini, H. Miao, D. Sayre, D.A. Shapiro, J.C.H. Spence, and D. Starodub. 2009. An assessment of the resolution limitation due to radiation-damage in X-ray diffraction microscopy. J. Electron Spectrosc. Relat. Phenom. 170: 4–12.

6. Henke, B.L., E.M. Gullikson, and J.C. Davis. 1993. X-Ray Interactions: Photoabsorption, Scattering, Transmission, and Reflection at E = 50-30,000 eV, Z = 1-92. At. Data Nucl. Data Tables. 54: 181–342.

7. Matlab R2012a. The MathWorks, Natick, MA.

8. van Heel, M., and M. Schatz. 2005. Fourier shell correlation threshold criteria. J. Struct. Biol. 151: 250–262.